ACS NANO
Cite This: ACS Nano 2018, 12, 10317−10326
www.acsnano.org

ARTICLE

Ultrathin Trilayer Assemblies as Long-Lived Barriers against Water and Ion Penetration in Flexible Bioelectronic Systems

Enming Song,[†,‡,&] Rui Li,[§,&] Xin Jin,[∥] Haina Du,[‡] Yuming Huang,[‡] Jize Zhang,[‡] Yu Xia,[‡] Hui Fang,[⊥] Yoon Kyeung Lee,[#] Ki Jun Yu,[⊗] Jan-Kai Chang,[†] Yongfeng Mei,[▽] Muhammad A. Alam,[∥] Yonggang Huang,[○] and John A. Rogers*[,†,‡,◆]

[†]Center for Bio-Integrated Electronics, Northwestern University, Evanston, Illinois 60208, United States
[‡]Frederick Seitz Materials Research Laboratory, Department of Materials Science and Engineering, University of Illinois at Urbana−Champaign, Urbana, Illinois 61801, United States
[§]State Key Laboratory of Structural Analysis for Industrial Equipment, Department of Engineering Mechanics, and International Research Center for Computational Mechanics, Dalian University of Technology, Dalian 116024, China
[∥]School of Electrical and Computer Engineering, Purdue University, West Lafayette, Indiana 47907, United States
[⊥]Department of Electrical and Computer Engineering, Northeastern University, Boston, Massachusetts 02115, United States
[#]Department of Materials Science and Engineering, Seoul National University, Seoul 08826, Republic of Korea
[⊗]School of Electrical and Electronic Engineering, Yonsei University, Seoul 03722, Republic of Korea
[▽]Department of Materials Science, Fudan University, Shanghai 200433, China
[○]Department of Mechanical Engineering, Civil and Environmental Engineering, and Materials Science and Engineering, Northwestern University, Evanston, Illinois 60208, United States
[◆]Departments of Materials Science and Engineering, Biomedical Engineering, Neurological Surgery, Chemistry, Mechanical Engineering, Electrical Engineering and Computer Science, Simpson Querrey Institute for Nano/Biotechnology, Northwestern University, Evanston, Illinois 60208, United States

Supporting Information

ABSTRACT: Biomedical implants that incorporate active electronics and offer the ability to operate in a safe, stable fashion for long periods of time must incorporate defect-free layers as barriers to biofluid penetration. This paper reports an engineered material approach to this challenge that combines ultrathin, physically transferred films of silicon dioxide (t-SiO_2) thermally grown on silicon wafers, with layers of hafnium oxide (HfO_2) formed by atomic layer deposition and coatings of parylene (Parylene C) created by chemical vapor deposition, as a dual-sided encapsulation structure for flexible bioelectronic systems. Accelerated aging tests on passive/active components in platforms that incorporate active, silicon-based transistors suggest that this trilayer construct can serve as a robust, long-lived, defect-free barrier to phosphate-buffered saline (PBS) solution at a physiological pH of 7.4. Reactive diffusion modeling and systematic immersion experiments highlight fundamental aspects of water diffusion and hydrolysis behaviors, with results that suggest lifetimes of many decades at physiological conditions. A combination of ion-diffusion tests under continuous electrical bias, measurements of elemental concentration profiles, and temperature-dependent simulations reveals that this encapsulation strategy can also block transport of ions that would otherwise degrade the performance of the underlying electronics. These findings suggest broad utility of this trilayer assembly as a reliable encapsulation strategy for the most demanding applications in chronic biomedical implants and high-performance flexible bioelectronic systems.

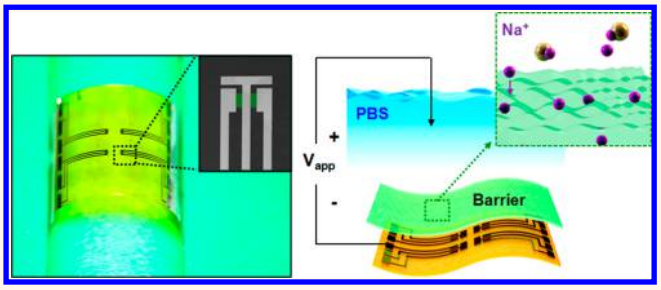

continued...

Received: July 23, 2018
Accepted: October 3, 2018
Published: October 3, 2018

DOI: 10.1021/acsnano.8b05552
ACS Nano 2018, 12, 10317−10326

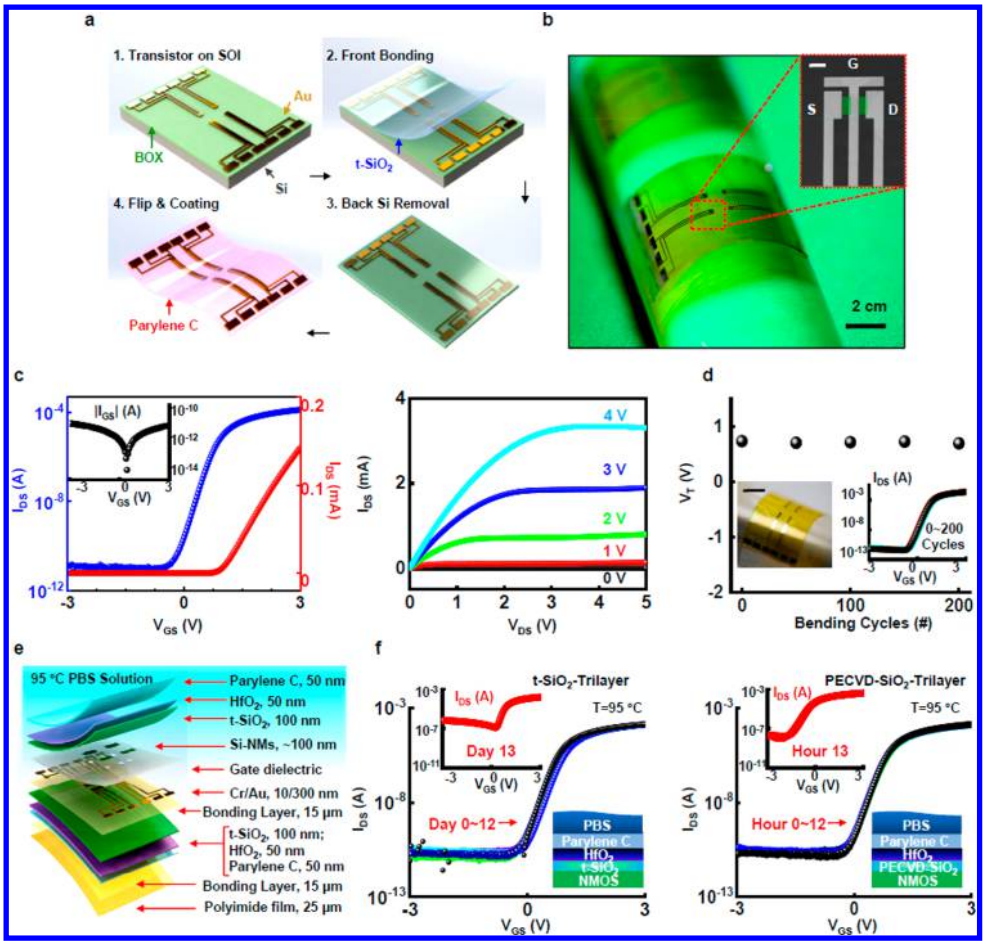

Figure 1. An ultrathin, trilayer of Parylene C, HfO_2, and t-SiO_2 provides the basis for a dual-side encapsulation strategy for flexible electronic implants. (a) Scheme for fabricating flexible electronic structures that incorporate silicon transistors: 1. Fabrication of a 2 × 2 array of transistors on an SOI wafer; 2. Pressure bonding the top surface of this wafer, face down, onto a t-SiO_2 layer that is coated with a thin film of polyimide; 3. Removal of the silicon handle wafer by dry etching; 4. Peeling the flexible device from the substrate; conformally coating with ALD HfO_2 and CVD Parylene C. (b) Optical image of samples produced in this manner with a trilayer barrier (Parylene C/HfO_2/t-SiO_2) on both sides. The upper inset shows a single test transistor with a scale bar of 200 μm. (c) Left: transfer characteristics plotted in both linear (red) and semilog scales (blue), at a supply voltage V_{DS}= 0.1 V. The inset shows gate leakage current. Right: Current−voltage characteristics, for V_G from 0 to 4 V with 1 V steps. (d) Results of bending tests of the NMOS transistor with Parylene C/HfO_2/t-SiO_2 trilayer barrier. The insets are optical images of a 2 × 2 transistor array with 1 cm bending radius and transfer characteristics before/after 200 bending cycles. (e) Schematic exploded-view illustration of the material stack for a 2 × 2 array of NMOS transistors. (f) Transfer characteristics collected during immersion in PBS solution at pH 7.4 and 95 °C, with Parylene C/HfO_2/t-SiO_2 (left) and Parylene C/HfO_2/PECVD-SiO_2 (right) barriers, respectively, as a comparison. The upper insets show that devices fail catastrophically at their corresponding lifetimes (Day 13 of Parylene C/HfO_2/t-SiO_2 and hour 13 of Parylene C/HfO_2/PECVD-SiO_2). The lower insets are schematic illustrations of the NMOS transistor stack.

KEYWORDS: *ultrathin encapsulation, flexible bioelectronics, chronic implant, reactive diffusion modeling, ion diffusion*

The emergence of high-performance flexible bioelectronic systems[1−8] with long-term operational stability when completely immersed in biofluids represents a breakthrough in biological interface engineering, with powerful capabilities of value in academic research and biomedical practice. Recent advances allow the construction of bioelectronic technologies with mechanical properties and geometrical shapes similar to those of targeted biological systems.[9−12] Such platforms can conform to the dynamic surfaces of targeted tissues as minimally invasive interfaces that also support levels of electronic performance and functionality associated with conventional wafer-based integrated circuits.[13−17] Some of the most sophisticated embodiments involve compliant sheets for multiplexed electrophysiological mapping on cardiac tissues[18−22] and on the surfaces of the brain.[23−26] Long-term operation *in vivo* requires isolation of the underlying backplane electronics from surrounding biofluids, to avoid leakage currents into adjacent tissues and corrosion of the active devices.

A key feature of these systems, then, is in the barrier layers, where targeted lifetimes for prevention of biofluid penetration can reach decades, or more, for certain envisioned applications in humans. The constituent materials must be biocompatible, with exceptionally low water/ion permeability and with uniform, thin film geometries to enable low flexural rigidity and large area coverage. Conventional means for forming surface coatings,[27−33] such as spin-casting, chemical vapor deposition (CVD), atomic layer deposition (ALD), physical vapor deposition (PVD), and others, typically fail to yield films that

DOI: 10.1021/acsnano.8b05552
ACS Nano 2018, 12, 10317−10326

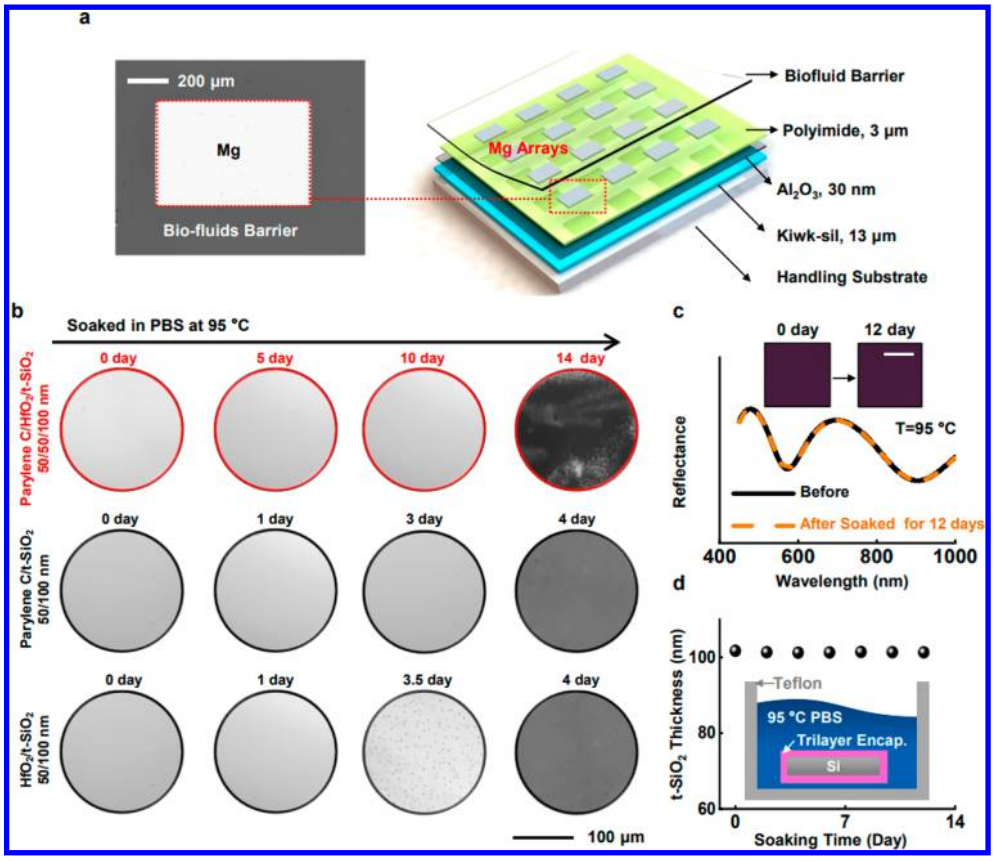

Figure 2. Accelerated soak tests and comparisons among different encapsulation strategies. (a) Top-view (left) and exploded-view (right) illustration of the layer configuration for accelerated soak tests that use arrays of Mg pads as indicators of water penetration. (b) Comparison results for accelerated immersion tests that involve immersion in PBS solution at pH 7.4 and 95 °C. Lifetimes corresponding to Parylene C/HfO_2/t-SiO_2, Parylene C/t-SiO_2 and HfO_2/t-SiO_2 are 14, 4, and 3.5 days, respectively. (c) Optical properties of a trilayer of Parylene C/HfO_2/t-SiO_2 before (black)/after (orange) 12-day soaking in PBS solutions at T = 95 °C. Insets show top-view optical images of trilayer barrier on a silicon wafer before/after soaking. The scale bar corresponds to a length of 1 cm. (d) Real-time measurements of thickness of t-SiO_2 during soak tests. Inset shows the trilayer at the surface/edges of a silicon wafer during accelerated soak tests.

meet the essential requirements because of either intrinsic limitations in the materials or extrinsic effects associated with grain boundaries, pinhole defects, or incomplete coverage of underlying surface topography. A recently reported alternative approach uses physically transferred layers of SiO_2 thermally grown on the polished surfaces of device-grade silicon wafers.[34] The intrinsic, defect-free properties (due to the nature of growth process and the perfection of the growth substrate), the ultralow water permeability, and the transfer procedures enable use of ultrathin, bendable layers of this form of SiO_2 (t-SiO_2) as a robust barrier layer for flexible bioelectronic systems. Representative results[35] include the application of films of t-SiO_2 with thicknesses less than one micron as barrier layers and simultaneously as capacitive measurement interfaces for electophysiological mapping arrays that use flexible silicon nanomembrane (Si-NM) transistors for multiplexing and buffering on a per-channel basis.

Here, the rate of hydrolysis of t-SiO_2 defines the limiting time scale (~100 nm/day over 95 °C)[34] for stable operation. A consequent challenge is that reductions in thickness improve the mechanics and enhance the capacitive coupling, yet decrease the lifetimes. Additionally, some species of ions in biofluids can diffuse through t-SiO_2, thereby degrading certain properties of the underlying transistors.[36] The addition of a capping layer of a material such as SiN_x can partially address these limitations.[37,38] Nevertheless, the ultrathin geometries and the unavoidable pinholes/defects that can form during deposition of such coatings typically lead to leakage currents and biofluid penetration.[34,37,39] These concerns motivate the pursuit of further improvements in schemes for encapsulation.

The following results outline a trilayer assembly that combines t-SiO_2, ALD-deposited HfO_2 and Parylene C layers formed by CVD for encapsulation, along with methods for device integration and system-level examples of such stacks in representative devices. The resulting barrier structure can be integrated across the surfaces of high-performance, flexible electronic systems, with excellent size scalability (over an area at any wafer size), good biocompatibility, defect-free interfaces, and projected lifetimes that extend over decades in the human body, even at thicknesses of only a few tens of nanometers. Accelerated soak tests of active devices and comparative evaluations against various other encapsulation strategies illustrate that such trilayers can provide robust biofluid barrier in ultrathin forms, with characteristics that exceed those of other material systems by orders of magnitude. Systematic experiments reveal the essential material properties and the ultimate failure mechanisms. Reactive diffusion modeling suggests that the capping layers (HfO_2 and Parylene C) can effectively slow the rates of water diffusion and the hydrolysis reactions of the underlying t-SiO_2, thereby yielding stable, long-term operation in implantable bioelectronic systems. Additional ion drift-diffusion tests with active electronics, depth-dependence

DOI: 10.1021/acsnano.8b05552
ACS Nano 2018, 12, 10317−10326

measurements of ion concentrations and temperature-dependent simulations demonstrate that this trilayer also provides superior capabilities in blocking ion transport driven by electrical bias. The results create significant opportunities in chronic operation of the most advanced types of flexible, biointegrated systems with active electronic functionality.

RESULTS AND DISCUSSION

The overall encapsulation system consists of an ultrathin stack of Parylene C/HfO_2/t-SiO_2 (50/50/100 nm), uniformly covering the top and/or bottom surfaces of implanted electronic platforms, with biocompatible properties.[40,41] The trilayer serves not only as an excellent biofluid barrier against water/ion penetration into the underlying active electronics but also as a capacitive interface for biophysical or biochemical measurement. Recent methods in semiconductor processing and transfer printing enable the formation of high-performance flexible electronic systems that incorporate this barrier structure (Figure 1a). A sequence of fabrication steps appears in Figure 1a. The first defines arrays of Si n-channel metal-oxide semiconductor (NMOS) transistors on a silicon-on-insulator (SOI) wafer. A bonding process joins the device side onto a preformed trilayer structure (Parylene C/HfO_2/t-SiO_2, 50/50/100 nm), with the t-SiO_2 side against a polymer film/glass plate as a temporary support. Dry-etching techniques remove the silicon wafer and stop at the back surface of buried-oxide (BOX, 100 nm; t-SiO_2) layer of the SOI platform. Conformal coatings of HfO_2 (50 nm) and Parylene C (50 nm) formed by ALD and CVD, respectively, yield ultrathin capping layers on the exposed t-SiO_2. Peeling the system from the glass substrate yields a piece of flexible electronics encapsulated by trilayers of Parylene C/HfO_2/t-SiO_2 on the front and back sides. Details appear in the Methods.

This encapsulation strategy can scale easily to sizes limited only by the dimensions of the silicon wafer (current maximum size: ~450 mm diameter). Figure 1b shows an optical image of an encapsulated system that consists of a 2 × 2 array of transistors, wrapped around a cylindrical surface. The scanning electron microscope (SEM) image in the inset shows a set of n-type transistors (channel length L = 17 μm, width W = 200 μm, thickness t = 100 nm). Figure 1c summarizes the electrical properties of a representative transistor, in which the on/off ratio and electron mobility are ~10^8 and ~500 $cm^2\ V^{-1}$, respectively, as calculated from standard field effect transistor models (see Supporting Information).[35] Mechanical bending tests in Figure 1d illustrate outstanding levels of robustness and flexibility. For ~1 cm bending radius (left inset of Figure 1d), the device performance remains unchanged after 200 cycles of bending/unbending, as shown in the right inset of Figure 1d.

A schematic illustration of the trilayer, Parylene C (biofluid side)/HfO_2/t-SiO_2 (device side), appears as an exploded view in Figure 1e. Results of tests of transistors during complete immersion in PBS solution at a pH of 7.4 are in Figure 1f, accelerated by high temperatures (95 °C), in the form of transfer characteristics of a typical n-type transistor. As shown in Figure 1f (left), these transistors, with trilayer barrier (Parylene C/HfO_2/t-SiO_2, 50/50/100 nm), exhibit stable performance until failure due to leakage currents that appear on Day 13 (inset). By comparison, a related trilayer of Parylene C/HfO_2/PECVD-SiO_2, 50/50/100 nm, fails catastrophically after only 13 hours (Figure 1f, right) because of pinholes in the PECVD SiO_2.[34] The lower insets show the layer configurations associated with the soak tests. As additional comparisons, bilayer barriers of HfO_2/t-SiO_2 (50/100 nm) and Parylene C/t-SiO_2 (50/100 nm) as in Figure S1, Supporting Information, also fail quickly at 3.5 days and 4 days (details are in Methods), respectively. The combination of Parylene C/HfO_2/t-SiO_2 offers a superior long-term encapsulation strategy.

As a means for visualizing patterns of water penetration, thin films of magnesium (Mg) serve as test structures to replace the transistors, as shown in Figure 2. Here, electron-beam-evaporated arrays of pads of Mg (length = 300 μm, width = 150 μm, thickness = 300 nm) react with water that passes through barrier layers coated or transferred on top (Figure 2a) according to $Mg + 2H_2O \rightarrow Mg(OH)_2 + H_2$, to generate visible signatures observable by optical microscopy. A schematic illustration of the experimental setup appears in Figure 2a (right), with an optical image of a set of Mg pads (left), all of which are immersed in PBS solution at 95 °C. Observations show that the Mg layer dissolves quickly (usually within hours) across the entire region of interest after the appearance of an initial defect. In the following, the lifetime corresponds to the period between initial immersion and observation of the first defect by optical microscopy. Details are in Methods.

Figure 2b displays results of accelerated soak tests with the trilayer of Parylene C/HfO_2/t-SiO_2, and bilayers of Parylene C/t-SiO_2 and HfO_2/t-SiO_2. Here, t-SiO_2 layers (device side) serve as pinhole-free water barriers to prevent water permeation, and capping layers (PBS side) reduce the rate of hydrolysis of the underlying t-SiO_2. Specifically, the bilayer systems (Parylene C/t-SiO_2, 50/100 nm and HfO_2/t-SiO_2, 50/100 nm) have lifetimes of only 4 days and 3.5 days, with failures in a "bulk" (spatially uniform reaction with the Mg) and a "pinhole" (localized reaction) mode, respectively, corresponding to water permeation across the entire polymeric layer (parylene) or penetration through isolated, pinhole defects (HfO_2). These findings motivate a trilayer design that combines key characteristics of both types of materials, to retard water penetration at the locations of pinhole-defects. As shown in Figure 2b, the trilayer of Parylene C/HfO_2/t-SiO_2 (50/50/100 nm) significantly extends the lifetime, where failure occurs with the emergence of dense patterns of defects after 14 days. The lifetime assessed in this manner is consistent with the transistor-performance results in Figure 1f (left). In the same manner, Table S1 (Supporting Information) summarizes a profile of other candidate structures for encapsulation, including various materials, thicknesses and single/multilayer configurations, etc (see details in Methods). In addition, Table S2 and Figure S2 (Supporting Information) highlight various properties of different polymer-based barriers with t-SiO_2 layers, and the superiority of Parylene C, consistent with findings in previous reports.[37] Of all of the examined single/multilayer systems, the lifetime of the trilayer (Parylene C/HfO_2/t-SiO_2) is the longest by a significant amount. Compared with PBS, other simulated biofluids, such as artificial perspiration (Pickering Laboratories), show slower rates of dissolution of the t-SiO_2 layer,[42] as the basis of trilayer assemblies (Figure S3 in Supporting Information).

Figure 2c,d summarize the optical properties of such trilayer structure, before/after the soak tests. Figure 2c is the optical reflectance (Mprobe, SemiconSoft, USA) of the Parylene/HfO_2/t-SiO_2 (50/50/100 nm) trilayer before/after a 12-day soaking test in PBS solution at 95 °C. The reflectance of before (black) and after (yellow) remains unchanged in a wavelength range from 450 to 1000 nm. The two top-view optical images in the insets indicate no apparent change in color. Studies of the t-SiO_2 layer thickness of this system provide additional details, as shown in Figure 2d. The inset displays a schematic illustration of

DOI: 10.1021/acsnano.8b05552
ACS Nano 2018, 12, 10317−10326

a Si wafer coated with a trilayer (Parylene/HfO_2/t-SiO_2, 50/50/100 nm) completely immersed in PBS at 95 °C, without any exposed edges. The thickness of the t-SiO_2 layer remains almost the same during continuous soaking. The corresponding SEM image shows the cross-sectional profile, with a thickness of ~100 nm of t-SiO_2 layer, after soaking for 12 days in Figure S4, Supporting Information. The results suggest the eventual failure follows from slow hydrolysis of the t-SiO_2 due to water penetration through defects in the capping layers.

Figure 3 summarizes the results of theoretical modeling of reactive diffusion for the hydrolysis of t-SiO_2 with capping layers

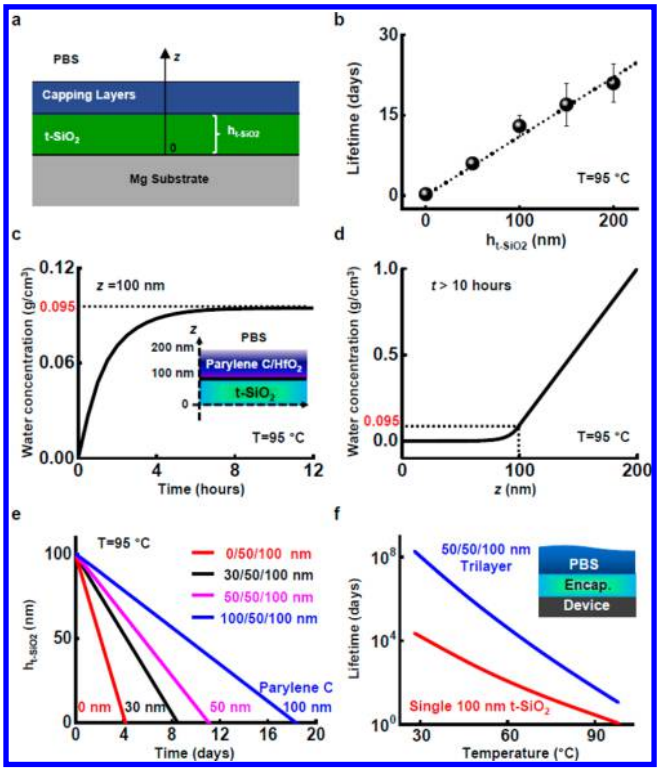

Figure 3. Theoretical modeling of reactive diffusion for the hydrolysis of t-SiO_2 with polymer/HfO_2 capping layers. (a) Schematic illustration of the model. (b) Simulated (line) and measured (symbols) lifetimes of a Parylene C/HfO_2/t-SiO_2 barrier with constant 50/50 nm thick Parylene C/HfO_2 layers and different thicknesses of underlying t-SiO_2 layers. (c) Distribution of water concentration as a function of soaking time at the interface between t-SiO_2 and Parylene C/HfO_2, where saturation is reached at ≈0.095 g cm^{-3} after ≈10 h. The inset shows a schematic illustration of the geometry. (d) Distribution of water concentration in both 100 nm thick t-SiO_2 and 50/50 nm thick Parylene C/HfO_2 layers after 10 h. (e) Changes in thickness of the t-SiO_2 in Parylene C/HfO_2/t-SiO_2 barriers with 50/100 nm thick HfO_2/t-SiO_2 and Parylene C with initial thicknesses of 0, 30, 50, and 100 nm. (f) Simulated temperature-dependent lifetimes of a layer of 100 nm thick t-SiO_2 w/o 50/50 nm thick Parylene C/HfO_2 capping layers. The inset shows a schematic illustration.

(Parylene C/HfO_2). Since the initial thickness of the structure is much smaller than the length and width, a 1D model can capture the hydrolysis process. As the reactions between water and Parylene C/HfO_2 can be ignored,[38] diffusion can be described by considering these two capping layers as an equivalent single layer of material. In combination with the t-SiO_2 layer, a bilayer barrier model (capping layer and t-SiO_2) on a pad of Mg is used, as illustrated in Figure 3a, where the z axis points upward along the thickness direction, with $z = 0$ at the bottom of the structure, that is, at the top of the Mg pad. For the equivalent capping layer (Parylene C/HfO_2), the equation of diffusion is

$$D_{\text{capping}}\frac{\partial^2 w}{\partial z^2} = \frac{\partial w}{\partial t} \quad (h_0 \le z \le h_0 + h_{\text{capping}}) \tag{1}$$

where D_{capping} is the equivalent diffusivity of water in the capping layer with thickness h_{capping} (the sum of polymer and HfO_2 thicknesses), w the water concentration that depends on time t and position z, and h_0 the initial thickness of the t-SiO_2. For the t-SiO_2, the reactive diffusion equation applies

$$D_{\text{t-SiO}_2}\frac{\partial^2 w}{\partial z^2} - k_{\text{t-SiO}_2} w = \frac{\partial w}{\partial t} \quad (0 \le z \le h_0) \tag{2}$$

where $D_{\text{t-SiO}_2}$ and $k_{\text{t-SiO}_2}$ are the diffusivity of water in t-SiO_2 and reaction constant between water and t-SiO_2, respectively. The constant water concentration w_0 (= 1 g cm^{-3}) at the top of the capping layer and zero water flux at the bottom of the t-SiO_2 require the boundary conditions: $w|_{z = h_0 + h_{\text{capping}}} = w_0$ and $\partial w/\partial z|_{z=0} = 0$. At the capping layer/t-SiO_2 interface, the continuity of both concentration and flux of water should be satisfied, which yields $w|_{z = h_0 - 0} = w|_{z = h_0 + 0}$ and $D_{\text{t-SiO}_2}\partial w/\partial z|_{z = h_0 - 0} = D_{\text{capping}}\partial w/\partial z|_{z = h_0 + 0}$. The initial condition of zero water concentration in the structure requires $w|_{t=0} = 0$ ($0 \le z \le h_0 + h_{\text{capping}}$).

The water concentration in the bilayer model can be analytically obtained by applying the method of separation of variables, which gives the thickness of the t-SiO_2, $h_{\text{t-SiO}_2}$, as a function of time (details appear in Methods). In the present study, a simplified expression of the thickness change of the t-SiO_2 is obtained as

$$\frac{h_{\text{t-SiO}_2}}{h_0} \approx 1 - \frac{t}{t_{\text{critical}}} \tag{3}$$

where

$$t_{\text{critical}} = \frac{q h_0 \rho_{\text{t-SiO}_2} M_{\text{H}_2\text{O}}}{w_0 M_{\text{t-SiO}_2}\sqrt{k_{\text{t-SiO}_2} D_{\text{t-SiO}_2}}\tanh\sqrt{\frac{k_{\text{t-SiO}_2} h_0^2}{D_{\text{t-SiO}_2}}}\left(1 + \frac{h_{\text{capping}}}{D_{\text{capping}}}\sqrt{k_{\text{t-SiO}_2} D_{\text{t-SiO}_2}}\tanh\sqrt{\frac{k_{\text{t-SiO}_2} h_0^2}{D_{\text{t-SiO}_2}}}\right)} \tag{4}$$

represents the time when the t-SiO_2 layer fully dissolves ($h_{\text{t-SiO}_2} = 0$), that is, the lifetime of the barrier. Here, q (= 2) is the number of water molecules reacting with each atom of t-SiO_2, $\rho_{\text{t-SiO}_2}$ is the mass density of t-SiO_2 (= 2.33 g cm^{-3}), and $M_{\text{H}_2\text{O}}$ (= 18 g mol^{-1}) and $M_{\text{t-SiO}_2}$ (= 60 g mol^{-1}) are the molar masses of water and t-SiO_2, respectively.

The $D_{\text{t-SiO}_2}$ and $k_{\text{t-SiO}_2}$ are determined by a single-layer reactive diffusion model[43] based on the dissolution tests of t-SiO_2 as $k_{\text{t-SiO}_2} = 1.8 \times 10^{-4}$ s^{-1} and $D_{\text{t-SiO}_2} = 1.3 \times 10^{-16}$ cm^2 s^{-1} at 95 °C. The constants at different temperatures can be obtained from the dissolution tests and the Arrhenius equation (details appear in Methods). D_{capping} at different temperatures are determined by the established bilayer model based on the lifetime tests of the trilayer Parylene C/HfO_2/t-SiO_2 (50/50/100 nm) at 90 °C (≈

DOI: 10.1021/acsnano.8b05552
ACS Nano 2018, 12, 10317−10326

30 days) and 95 °C (≈ 13.5 days) according to Arrhenius scaling, for example, $D_{capping} = 1.6 \times 10^{-16}$ cm^2 s^{-1} at 95 °C (see Methods).

Figure 3b plots the lifetime of the Parylene C/HfO_2/t-SiO_2 barrier as a function of the initial thickness of the t-SiO_2 in PBS solution at 95 °C, with 50/50 nm thick Parylene C/HfO_2 capping layers kept constant. The simulated (line) and measured (symbols) barrier lifetimes show good agreement, both reflecting an approximately linear relationship between the lifetime and t-SiO_2 thickness. Figure 3c predicts the distribution of water concentration as a function of soaking time at the interface (z = 100 nm) between the t-SiO_2 (100 nm) and the Parylene C/HfO_2 (50/50 nm) capping layer. The water concentration saturates at ≈0.095 g cm^{-3} after ≈10 hours, suggesting that reaction and diffusion reach equilibrium in a relatively short time. The distribution of water concentration along the thickness direction after saturation is shown in Figure 3d. The distribution is uniform in the t-SiO_2 and nonuniform in the capping layers, indicating that water diffusion in the capping layers is much slower than that in t-SiO_2. Therefore, the capping layers effectively slow the rates of hydrolysis of the t-SiO_2. Figure 3e predicts changes in the thickness of the t-SiO_2 layer when capped with HfO_2 (50 nm) and Parylene C at thicknesses of 0, 30, 50, and 100 nm. The results show a linear decrease in the thickness with time, as predicted by Equation 3. With the specific $k_{t\text{-}SiO_2}$, $D_{t\text{-}SiO_2}$ and $D_{capping}$ at different temperatures (see details in Methods), the temperature-dependent lifetimes of a single layer of t-SiO_2 (100 nm) and a trilayer of Parylene C/HfO_2/t-SiO_2 (50/50/100 nm) are obtained by each reactive diffusion model,[43] as shown in Figure 3f (the red and blue lines). According to the theoretical modeling, the trilayer design is expected to increase the lifetime projection at least by 3 orders of magnitude in 37 °C PBS solution compared with the case of single t-SiO_2, a result of which is also consistent with the experimental projections on measured hydrolysis rates of t-SiO_2.[34]

The previously described experiments and simulation results identify that water permeation and a slow hydrolysis process are essential causes of the eventual failure of the barrier structure. In addition to water, ions present in biofluids, mostly positive species such as Na^+, are also important to consider, as they can lead to unwanted electrostatic shifts in the characteristics of the underlying transistors (such as fluctuations in threshold voltage, V_T)[36] particularly when ions approaching the device regions. In this context, the barrier structure should not only prevent water-leakage but also block ionic transport. Figure 4a (left) schematically illustrates a 2 × 2 NMOS transistor array immersed in PBS solution at 95 °C and pH of 7.4, with an external electrical bias applied between transistor electrodes (source, drain, gate) and a platinum probe in PBS. The bias (V_{app}, 3 V) drives preferential flow of cations toward the Si NMOS transistors. The t-SiO_2, despite its excellent water-barrier properties, is a poor barrier to ions, particularly sodium in the presence of a positive electrical driving force,[37] as shown in Figure 4a (right). A capping layer of SiN_x can prevent penetration of sodium,[37,44] but its high rate of hydrolysis in biofluids (larger by orders of magnitude compared to that of t-SiO_2).[39]

Secondary-ion-mass-spectroscopy (SIMS) techniques yield information on the cross-sectional depth profile of [Na^+] in the t-SiO_2 with/without (w/o) integration into the trilayer construct (Parylene C/HfO_2/t-SiO_2), as shown in Figure 4b,c.

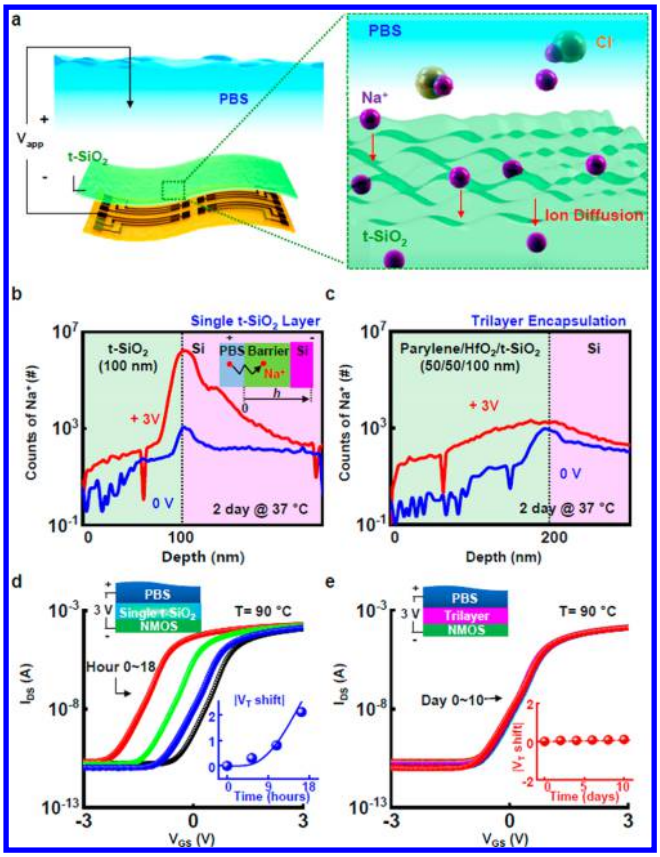

Figure 4. NMOS transistor performance with/without trilayer barrier in PBS solution at pH 7.4 and 90 °C. (a) Left: schematic illustration of the embedded NMOS devices in PBS solution under external electrical bias. Right: Sodium penetration occurs at the surface of the t-SiO_2. (b, c) Cross-sectional profile of [Na^+] at the t-SiO_2/Si interface under various V_{app} (0 V, 3 V) in single t-SiO_2 barrier (b) and trilayer barriers (c). The inset provides a one-dimensional diffusion illustration of the geometry. (d, e) Results of tests for (d) a 100 nm thick layer of t-SiO_2 and (e) a 50/50/100 nm thick trilayer of Parylene C/HfO_2/t-SiO_2 in PBS soak tests at 90 °C, with V_{app} = 3 V. Schematic illustrations of the samples and bias configurations appear in the upper insets. Lower insets show the shift of the threshold voltage as a function of time. The solid dots are experimental data.

The inset in Figure 4b shows a one-dimensional schematic illustration based of Na^+ penetration through the t-SiO_2 layer. With the Na^+ spreading toward t-SiO_2, a retardation of transport process occurs at the t-SiO_2/Si boundary where Na^+ diffusivity $D_{Na^+, SiO_2} \gg D_{Na^+, Si}$.[45−47] The results lead to [Na^+] accumulation at the interfaces of t-SiO_2/Si, thereby yielding a concentration peak (detailed analysis appears in Supporting Information), which occurs at depths of 100 and 200 nm in single t-SiO_2 barrier and trilayer barrier structures, respectively. For a 100 nm thick single layer of t-SiO_2 (Figure 4b), the positive V_{app} (3 V, the red line) increases the [Na^+] at the interface of t-SiO_2/Si devices by a factor of ~10^4 relative the zero bias condition (0 V, the blue line) after soaking in PBS solution at 37 °C for 2 days. By contrast, for the trilayer barrier (Parylene C/HfO_2/t-SiO_2, 50/50/100 nm), as in Figure 4c, the [Na^+] stabilizes and saturates at the t-SiO_2/Si interfaces at concentrations that are identical w/o the 3 V V_{app} (the blue and red lines). Compared to the case of a single layer of t-SiO_2, the trilayer structure retards ion diffusion effectively due to the presence of the capping layers.

DOI: 10.1021/acsnano.8b05552
ACS Nano 2018, 12, 10317−10326

Measurements on NMOS transistors w/o trilayer barriers in ion drift-diffusion tests appear in Figure 4d,e (V_{app} = 3 V and T = 90 °C), respectively. The upper insets illustrate the configurations of single t-SiO_2 layers (100 nm) and trilayer (Parylene C/HfO_2/t-SiO_2, 50/50/100 nm). For the former case, as shown in Figure 4d, ions accumulate at the t-SiO_2/Si interfaces in proximity to the channel regions of the transistors, thereby shifting/degrading the switching characteristics.[36,44] The corresponding Na^+ concentration distributions are in Figure S5a, Supporting Information, also consistent with Figure 4b. Specifically, the formation of a layer of positive ions creates an electrical field that adds with that associated with the gate electrode, the result of which is an increase in the magnitude of the negative V_G to switch the transistors to their on state.[44] As displayed in the lower inset of Figure 4d, the software simulation[37] (Sentaurus Technology Computer Aided Design) yields numerical estimates of the shift in V_T during soaking for 18 h in 90 °C PBS solution at V_{app} = 3 V. The results (the blue line) agree with the experimental data (blue dots). Details of calculation are in Figure S5b (Supporting Information). As in Figure 4e, key characteristics of transistors with trilayer barriers remain unchanged during soak tests with the same condition. Specifically, the V_T does not drift (inset of Figure 4e). Thus, the trilayer system serves simultaneously as barriers to both water and ion penetration.

CONCLUSIONS

The materials and integration strategies reported here suggest that ultrathin, transferred trilayer stacks of Parylene C, HfO_2, and t-SiO_2 can serve as robust water and ion barrier structures for flexible bioelectronic systems. Comparative evaluations of the barrier properties of this system with those that involve other materials and deposition methods establish its attractive features. Detailed experimental studies and theoretical modeling results highlight underlying materials aspects associated with water and ion permeation. The findings suggest a promising, scalable encapsulation approach that can be applied to nearly all classes of thin, flexible bioelectronic systems, with projected survivability of many years as implantable devices.

METHODS

Methods for Fabricating Arrays of Transistors Encapsulated with t-SiO_2. The fabrication began with device processing in a layer-by-layer fashion on a preformed barrier layer. Specifically, photolithographic methods and etching techniques formed phosphorus doped (PH-1000N Source, Saint Gobain, 1000 °C for 7 min) Si-NMs on a SOI wafer (100 nm thick Si-NMs). Oxidation (1150 °C for 16 min) and ALD deposition yielded 40/15 nm thick layers of t-SiO_2 and Al_2O_3 as the gate dielectric stacks. Buffered oxide etchant (BOE) opened the source/drain contact regions. Deposition of Cr/Au (10/300 nm) layers by electron beam evaporation defined the electrodes and interconnects. Simultaneously, an oxidized silicon wafer (100 nm thick t-SiO_2, 200 μm thick Si wafer, University Wafer) with a bilayer coating of Parylene C/HfO_2 (50/50 nm) formed by CVD/ALD was bonded to a thin polyimide film (Kapton, DuPont, 13 μm) supported by a glass plate coated with a thin layer of poly(dimethylsiloxane) (PDMS, 10 μm). Inductively coupled plasma reactive ion etching (ICP-RIE, Surface Technology System) with a gas flow of SF_6/O_2 40/3 sccm at a pressure of 50 mT removed the silicon wafer. A transfer process then bonded the device side of the other wafer to the exposed t-SiO_2 layer. The bonding used a coating of polyimide (PI-2545, HD MicroSystems, 1.5 μm) and a separate adhesive (Kwik-sil, World Precision Instruments, 13 μm). ICP-RIE removed the silicon wafer of the SOI platform and terminated at the BOX, leaving a ~100 nm thick layer of t-SiO_2 (see Figure S6, Supporting Information). Additional steps of depositing layers of HfO_2 (ALD, 200 °C, Ultratech/Cambridge Nanotech) and/or Parylene C (CVD, 135 °C, SCS Parylene Deposition System) formed various types of capping layers on the t-SiO_2 e.g. Parylene C/HfO_2/t-SiO_2, 50/50/100 nm; Parylene C/t-SiO_2, 50/100 nm; HfO_2/t-SiO_2, 50/100 nm, as shown in Figure 1f (left), Figures S1a,b in Supporting Information, respectively. Photolithography defined areas to allow creation of openings for electrical contact by ICP-RIE with SF_6/O_2. Finally, a laser-cutting step allowed the device to be peeled from the handle substrate, as displayed with the exploded view in Figure 1e.

Integration with the trilayer of Parylene C/HfO_2/PECVD-SiO_2 involved releasing, retrieving and transferring doped Si-NMs onto a glass substrate, precoated with PI-2545 layer (~ 1.5 μm thick) as adhesive layers.[48] To avoid thermal damage to the transferred structure, a bilayer dielectric of PECVD-SiO_2/ALD-Al_2O_3 (30/13 nm) served as the gate dielectric materials. Subsequent formation of a trilayer structure on the device side, including PECVD-SiO_2 (350 °C, PECVD-Trion Orion Minilock), HfO_2, and Parylene C in a layer-by-layer fashion, yielded a barrier structure for the transistors.

Accelerated Soak Tests for NMOS Transistors. Measurements of the electrical performance of transistors with different types of barriers involved continuous soak tests in PBS solutions (pH = 7.4) at a temperature of 95 °C. Device electrodes were biased with and without the application of a voltage relative to a Pt reference electrode inserted into the PBS solution. A PDMS well structure (~2 cm in depth) physically bonded onto the ultraviolet ozone (UVO) treated surfaces of the barrier layers confined the PBS solution to the device areas, and away from the edges of the substrate. The measured lifetimes of Parylene C/HfO_2/t-SiO_2 (50/50/100 nm), Parylene C/t-SiO_2 (50/100 nm), and HfO_2/t-SiO_2 (50/100 nm) barrier constructs were 13, 3, and 3.5 days, respectively, as shown in Figure 1f (left), Figure S1a,b, Supporting Information.

Mg Tests for Evaluation of Water Barrier Performance. Photolithography and electron beam evaporation defined arrays of pads of Ti/Mg (5/300 nm) on a clean t-SiO_2 wafer (100 nm thick t-SiO_2). Subsequently, various deposition methods produced different kinds of barrier materials for accelerated soak tests. As shown in Tables S1, Supporting Information, formation of t-SiO_2 barrier followed procedures similar to those described previously in Figure 1a. ALD formed metal oxide layers (i.e., Al_2O_3, HfO_2, and TiO_2). CVD and low-pressure chemical vapor deposition (LPCVD) yielded Parylene C and SiN_x layers (~800 °C, Rogue Valley Microdevices), respectively. Spin coating defined layers of solution-processable polymers (e.g., SU-8, PMMA, PI-2545). Metal layers were deposited by electron beam evaporation. Tables S1 and S2, Supporting Information summarize all of the results. To summarize, the investigated organic films are water-permeable but they do not exhibit pinholes. The result is that these materials can reduce the rate of water diffusion on average, but they fail to prevent penetration. Inorganic layers, such as ALD-grown layers, metal layers, and SiN_x films, are much less permeable, but they all have pinholes. Such defects could, potentially, be reduced by improving the levels of particulate control and the deposition conditions. The results presented here are typical of those achievable in academic cleanroom facilities. Inorganic/organic multilayer structures provide superior performance compared with single layers with similar total thickness, due to a combination of advantages of each material.

Reactive Diffusion Model for the Hydrolysis of t-SiO_2 with Polymer/HfO_2 Capping Layers. Theoretical modeling of reactive diffusion for the hydrolysis of polymer/HfO_2/t-SiO_2 barriers used a bilayer model approximation (capping layer and t-SiO_2), as illustrated in Figure 3. By applying the method of separation of variables to the equation of diffusion for the equivalent capping layer (polymer/HfO_2) and to the equation of reactive diffusion for the t-SiO_2, incorporating both the boundary and continuity conditions, the water concentration distributed in the structure was analytically obtained as

$$w = w_0\left[\sum_{n=1}^{\infty} C_n \exp(-\lambda_n t) f_n(z) + g(z)\right] \quad (5)$$

where

DOI: 10.1021/acsnano.8b05552
ACS Nano 2018, 12, 10317−10326

$$f_n(z) = \begin{cases} \sin\left(\sqrt{\frac{\lambda_n}{D_{capping}}}h_{capping}\right)\cos\left(\sqrt{\frac{\lambda_n - k_{t\text{-}SiO_2}}{D_{t\text{-}SiO_2}}}z\right), \\ 0 \le z \le h_0 \\ \cos\left(\sqrt{\frac{\lambda_n - k_{t\text{-}SiO_2}}{D_{t\text{-}SiO_2}}}h_0\right)\sin\left[\sqrt{\frac{\lambda_n}{D_{capping}}}(h_0 + h_{capping} - z)\right], \\ h_0 \le z \le h_0 + h_{capping} \end{cases} \quad (6)$$

and

$$g(z) = \begin{cases} F\cosh\left(\sqrt{\frac{k_{t\text{-}SiO_2}}{D_{t\text{-}SiO_2}}}z\right), & 0 \le z \le h_0 \\ 1 - G(h_0 + h_{capping} - z), & h_0 \le z \le h_0 + h_{capping} \end{cases} \quad (7)$$

with

$$F = \frac{1}{\sqrt{k_{t\text{-}SiO_2}D_{t\text{-}SiO_2}}\frac{h_{capping}}{D_{capping}}\sinh\sqrt{\frac{k_{t\text{-}SiO_2}h_0^2}{D_{t\text{-}SiO_2}}} + \cosh\sqrt{\frac{k_{t\text{-}SiO_2}h_0^2}{D_{t\text{-}SiO_2}}}}$$

$$G = \frac{1}{\frac{D_{capping}}{\sqrt{k_{t\text{-}SiO_2}D_{t\text{-}SiO_2}}}\coth\sqrt{\frac{k_{t\text{-}SiO_2}h_0^2}{D_{t\text{-}SiO_2}}} + h_{capping}} \quad (8)$$

λ_n (n = 1,2,3,....) were determined by the transcendental equation

$$\tan\sqrt{(\lambda - k_{t\text{-}SiO_2})h_0^2/D_{t\text{-}SiO_2}}\tan\sqrt{\lambda h_{capping}^2/D_{capping}} = \sqrt{\lambda D_{capping}/[(\lambda - k_{t\text{-}SiO_2})D_{t\text{-}SiO_2}]}$$

, which resulted from the continuity of both concentration and flux of water at the capping layer/t-SiO_2 interface. Applying the initial condition of zero water concentration in the structure yielded $\sum_{n=1}^{\infty} C_n f_n(z) + g(z) = 0$. According to orthogonality of the eigenfunctions, that was, $\int_0^{h_0 + h_{capping}} f_m(z) f_n(z) dy = 0$ for $m \neq n$, we obtained $C_n = -\int_0^{h_0 + h_{capping}} f_n(z) g(z) dy / \int_0^{h_0 + h_{capping}} f_n^2(z) dy$, yielding

$$C_n = \frac{-2\sqrt{\frac{D_{capping}}{\lambda_n}}\cos\left(\sqrt{\frac{\lambda_n - k_{t\text{-}SiO_2}}{D_{t\text{-}SiO_2}}}h_0^2\right)}{\left\{h_0\sin^2\left(\sqrt{\frac{\lambda_n}{D_{capping}}}h_{capping}^2\right)\left[1 + \frac{\sin\left(2\sqrt{\frac{\lambda_n - k_{t\text{-}SiO_2}}{D_{t\text{-}SiO_2}}}h_0^2\right)}{2\sqrt{\frac{\lambda_n - k_{t\text{-}SiO_2}}{D_{t\text{-}SiO_2}}}h_0^2}\right] + h_{capping}\cos^2\left(\sqrt{\frac{\lambda_n - k_{t\text{-}SiO_2}}{D_{t\text{-}SiO_2}}}h_0^2\right)\left[1 - \frac{\sin\left(2\sqrt{\frac{\lambda_n}{D_{capping}}}h_{capping}^2\right)}{2\sqrt{\frac{\lambda_n}{D_{capping}}}h_{capping}^2}\right]\right\}} \quad (9)$$

The thickness of the dissolved t-SiO_2 was obtained by integrating $k_{t\text{-}SiO_2}wM_{t\text{-}SiO_2}h_0/(q\rho_{t\text{-}SiO_2}M_{H_2O})$ over both the time and thickness direction, with q = 2 according to $SiO_2 + 2H_2O \rightarrow Si(OH)_4$. Subtraction from h_0 of the integration gave the remaining thickness of t-SiO_2. By normalization, we had

$$\frac{h_{t\text{-}SiO_2}}{h_0} = 1 - \frac{w_0 M_{t\text{-}SiO_2}}{q\rho_{t\text{-}SiO_2}M_{H_2O}}k_{t\text{-}SiO_2}\left\{Gt\cdot\frac{\sinh\sqrt{\frac{k_{t\text{-}SiO_2}h_0^2}{D_{t\text{-}SiO_2}}}}{\sqrt{\frac{k_{t\text{-}SiO_2}h_0^2}{D_{t\text{-}SiO_2}}}} + \sum_{n=1}^{\infty}\frac{C_n}{\lambda_n}[1 - \exp(-\lambda_n t)]\sin\sqrt{\frac{\lambda_n}{D_{capping}}}h_{capping}^2\frac{\sin\sqrt{\frac{\lambda_n - k_{t\text{-}SiO_2}}{D_{t\text{-}SiO_2}}}h_0^2}{\sqrt{\frac{\lambda_n - k_{t\text{-}SiO_2}}{D_{t\text{-}SiO_2}}}h_0^2}\right\} \quad (10)$$

In the present study, the summation on the right-hand side of eq 10 was negligible such that a simplified equation was obtained, as given by eq 3.

The reaction constant $k_{t\text{-}SiO_2}$ and diffusivities $D_{t\text{-}SiO_2}$ and $D_{capping}$ at different temperatures were necessary for evaluation of the water barrier performances. Based on the Arrhenius equation, $k_{t\text{-}SiO_2} = k_0\exp(-E_A/RT)$, where E_A was the activation energy (= 1.32 eV),[34] R the universal gas constant (= 8.314 J K^{-1} mol^{-1}), and T the absolute temperature with Kelvin units; the pre-exponential factor k_0 was determined by using $k_{t\text{-}SiO_2}$ = 1.8 × 10^{-4} s^{-1} at 95 °C, which was obtained by a single-layer reactive diffusion model[43] based on the dissolution tests of t-SiO_2. $k_{t\text{-}SiO_2}$was thus obtained as $k_{t\text{-}SiO_2}$ = 2.1 × 10^{14} × exp(− 15313/T) s^{-1}. $D_{t\text{-}SiO_2}$ at different temperatures were obtained from the dissolution rates observed in the experiments based on the single-layer reactive diffusion model. For example, $D_{t\text{-}SiO_2}$ = 5.3 × 10^{-20} cm^2 s^{-1} at 37 °C, 9.5 × 10^{-18} cm^2 s^{-1} at 70 °C, and 1.3 × 10^{-16} cm^2 s^{-1} at 95 °C. For the equivalent capping layer (polymer/HfO_2), $D_{capping}$ at different temperatures were determined by the established model based on the lifetime tests. For 50/50/100 nm thick Parylene C/HfO_2/t-SiO_2, the lifetime tests gave ≈30 days at 90 °C and ≈13.5 days at 95 °C, which led to $D_{capping}$ = 10^(15.13−11381/T) cm^2 s^{-1} according to Arrhenius scaling. Figure S2 (Supporting Information) predicted the lifetimes of 100/50/100 nm thick polymer/HfO_2/t-SiO_2 barriers with different polymers in PBS solution at 95 °C, including PI, PMMA, SU-8, and Parylene C, corresponding to $D_{capping}$ = 6 × 10^{-16} cm^2 s^{-1}, 5 × 10^{-16} cm^2 s^{-1}, 5.5 × 10^{-16} cm^2 s^{-1}, and 1.4 × 10^{-16} cm^2 s^{-1}, respectively. The predictions agreed well with the experimental results shown in Table S2, Supporting Information.

ASSOCIATED CONTENT

Supporting Information

The Supporting Information is available free of charge on the ACS Publications website at DOI: 10.1021/acsnano.8b05552.

Details of field-effect-transistor modeling, Na^+ spatial distribution profiles and the theoretical analysis including ion diffusion; figures and tables that summarize the results of accelerated soak tests of NMOS transistors with different bilayer barriers, properties of various encapsulation strategies, lifetimes of polymer/HfO_2/SiO_2 barriers with different polymers, experimental demonstrations of barrier performance in different biofluids, the cross-sectional view of SEM images, and ion drift-diffusion simulation results (PDF)

AUTHOR INFORMATION

Corresponding Author

*E-mail: jrogers@northwestern.edu.

ORCID

Enming Song: 0000-0002-2658-904X
Hui Fang: 0000-0002-4651-9786
Jan-Kai Chang: 0000-0002-3056-1250
Yongfeng Mei: 0000-0002-3314-6108

DOI: 10.1021/acsnano.8b05552
ACS Nano 2018, 12, 10317−10326

John A. Rogers: 0000-0002-2980-3961

Author Contributions

[&]E.S. and R.L. contributed equally to this work.

Notes

The authors declare no competing financial interest.

ACKNOWLEDGMENTS

This work was supported by Defense Advanced Research Projects Agency Contract HR0011-14-C-0102, and the Center for Bio-Integrated Electronics. We acknowledge the use of facilities in the Micro and Nanotechnology Laboratory for device fabrication and the Frederick Seitz Materials Research Laboratory for Advanced Science and Technology for device measurement at the University of Illinois at Urbana−Champaign. R.L. acknowledges the support from the Young Elite Scientists Sponsorship Program by CAST (No. 2015QNRC001) and Opening Fund of State Key Laboratory of Nonlinear Mechanics, Chinese Academy of Sciences. X.J. And M.A.A. acknowledge the support from Lilly Endowment through the Wabash Heartland Innovation Network (WHIN) (grant number: 40001922). K.J.Y. acknowledges the support from the National Research Foundation of Korea (NRF-2017M1A2A2048880, NRF-2018M3A7B4071109) and the Yonsei University Future-leading Research Initiative of (RMS2 2018-22-0028).

REFERENCES

(1) Won, S. M.; Song, E.; Zhao, J.; Li, J.; Rivnay, J.; Rogers, J. A. Recent Advances in Materials, Devices, and Systems for Neural Interfaces. *Adv. Mater.* **2018**, *30*, 1800534.

(2) Fu, T. M.; Hong, G.; Viveros, R. D.; Zhou, T.; Lieber, C. M. Highly Scalable Multichannel Mesh Electronics for Stable Chronic Brain Electrophysiology. *Proc. Natl. Acad. Sci. U. S. A.* **2017**, *114*, E10046−E10055.

(3) Viventi, J.; Kim, D.-H.; Vigeland, L.; Frechette, E. S.; Blanco, J. A.; Kim, Y. S.; Avrin, A. E.; Tiruvadi, V. R.; Hwang, S.-W.; Vanleer, A. C.; Wulsin, D. F.; Davis, K.; Gelber, C. E.; Palmer, L.; Van der Spiegel, J.; Wu, J.; Xiao, J.; Huang, Y.; Contreras, D.; Rogers, J. A.; et al. Flexible, Foldable, Actively Multiplexed, High-Density Electrode Array for Mapping Brain Activity *In Vivo*. *Nat. Neurosci.* **2011**, *14*, 1599−1605.

(4) Jun, J. J.; Steinmetz, N. A.; Siegle, J. H.; Denman, D. J.; Bauza, M.; Barbarits, B.; Lee, A. K.; Anastassiou, C. A.; Andrei, A.; Aydın, Ç.; Barbic, M.; Blanche, T. J.; Bonin, V.; Couto, J.; Dutta, B.; Gratiy, S. L.; Gutnisky, D. A.; Häusser, M.; Karsh, B.; Ledochowitsch, P.; et al. Fully Integrated Silicon Probes for High-Density Recording of Neural Activity. *Nature* **2017**, *551*, 232−236.

(5) Yu, K. J.; Kuzum, D.; Hwang, S. W.; Kim, B. H.; Juul, H.; Kim, N. H.; Won, S. M.; Chiang, K.; Trumpis, M.; Richardson, A. G.; Cheng, H.; Fang, H.; Thompson, M.; Bink, H.; Talos, D.; Seo, K. J.; Lee, H. N.; Kang, S. K.; Kim, J. H.; Lee, J. Y.; et al. Bioresorbable Silicon Electronics for Transient Spatiotemporal Mapping of Electrical Activity from the Cerebral Cortex. *Nat. Mater.* **2016**, *15*, 782−791.

(6) Tian, B.; Cohen-Karni, T.; Qing, Q.; Duan, X. J.; Xie, P.; Lieber, C. M. Three-Dimensional, Flexible Nanoscale Field-Effect Transistors as Localized Bioprobes. *Science* **2010**, *329*, 830−834.

(7) Yan, Z.; Han, M.; Shi, Y.; Badea, A.; Yang, Y.; Kulkarni, A.; Hanson, E.; Kandel, M. E.; Wen, X.; Zhang, F.; Luo, Y.; Lin, Q.; Zhang, H.; Guo, X.; Huang, Y.; Nan, K.; Jia, S.; Oraham, A. W.; Mevis, M. B.; Kim, J.; et al. Three-Dimensional Mesostructures as High-Temperature Growth Templates, Electronic Cellular Scaffolds, and Self-Propelled Microrobots. *Proc. Natl. Acad. Sci. U. S. A.* **2017**, *114*, E9455−E9464.

(8) Kim, D.-H.; Lu, N.; Ma, R.; Kim, Y.-S.; Kim, R.-H.; Wang, S.; Wu, J.; Won, S. M.; Tao, H.; Islam, A.; Yu, K. J.; Kim, T.-i.; Chowdhury, R.; Ying, M.; Xu, L.; Li, M.; Chung, H.-J.; Keum, H.; McCormick, M.; Liu, P.; et al. Epidermal Electronics. *Science* **2011**, *333*, 838−843.

(9) Lipomi, D. J.; Vosgueritchian, M.; Tee, B. C.; Hellstrom, S. L.; Lee, J. A.; Fox, C. H.; Bao, Z. Skin-Like Pressure and Strain Sensors Based on Transparent Elastic Films of Carbon Nanotubes. *Nat. Nanotechnol.* **2011**, *6*, 788−792.

(10) Xu, S.; Zhang, Y.; Jia, L.; Mathewson, K. E.; Jang, K. I.; Kim, J.; Fu, H.; Huang, X.; Chava, P.; Wang, R.; Bhole, S.; Wang, L.; Na, Y. J.; Guan, Y.; Flavin, M.; Han, Z.; Huang, Y.; Rogers, J. A. Soft Microfluidic Assemblies of Sensors, Circuits, and Radios for the Skin. *Science* **2014**, *344*, 70−74.

(11) Nawrocki, R.; Matsuhisa, N.; Yokota, T.; Someya, T. 300-nm Imperceptible, Ultraflexible, and Biocompatible e-Skin Fit with Tactile Sensors and Organic Transistors. *Adv. Electron Mater.* **2016**, *2*, 1500452.

(12) Gao, W.; Emaminejad, S.; Nyein, H. Y.; Challa, S.; Chen, K.; Peck, A.; Fahad, H. M.; Ota, H.; Shiraki, H.; Kiriya, D.; Lien, D. H.; Brooks, G. A.; Davis, R. W.; Javey, A. Fully Integrated Wearable Sensor Arrays for Multiplexed *In Situ* Perspiration Analysis. *Nature* **2016**, *529*, 509−514.

(13) Wu, W.; Wang, L.; Li, Y.; Zhang, F.; Lin, L.; Niu, S.; Chenet, D.; Zhang, X.; Hao, Y.; Heinz, T. F.; Hone, J.; Wang, Z. L. Piezoelectricity of Single-Atomic-Layer MoS_2 for Energy Conversion and Piezotronics. *Nature* **2014**, *514*, 470−474.

(14) McAlpine, M. C.; Ahmad, H.; Wang, D.; Heath, J. R. Highly Ordered Nanowire Arrays on Plastic Substrates for Ultrasensitive Flexible Chemical Sensors. *Nat. Mater.* **2007**, *6*, 379−384.

(15) Kaltenbrunner, M.; Sekitani, T.; Reeder, J.; Yokota, T.; Kuribara, K.; Tokuhara, T.; Drack, M.; Schwödiauer, R.; Graz, I.; Bauer-Gogonea, S.; Bauer, S.; Someya, T. An Ultra-Lightweight Design for Imperceptible Plastic Electronics. *Nature* **2013**, *499*, 458−463.

(16) Lochner, C. M.; Khan, Y.; Pierre, A.; Arias, A. C. All-Organic Optoelectronic Sensor for Pulse Oximetry. *Nat. Commun.* **2014**, *5*, 5745.

(17) Son, D.; Lee, J.; Qiao, S.; Ghaffari, R.; Kim, J.; Lee, J. E.; Song, C.; Kim, S. J.; Lee, D. J.; Jun, S. W.; Yang, S.; Park, M.; Shin, J.; Do, K.; Lee, M.; Kang, K.; Hwang, C. S.; Lu, N.; Hyeon, T.; Kim, D.-H. Multifunctional Wearable Devices for Diagnosis and Therapy of Movement Disorders. *Nat. Nanotechnol.* **2014**, *9*, 397−404.

(18) Viventi, J.; Kim, D.-H.; Moss, J. D.; Kim, Y.-S.; Blanco, J. A.; Annetta, N.; Hicks, A.; Xiao, J. L.; Huang, Y.; Callans, D. J.; Rogers, J. A.; Litt, B. A Conformal, Bio-Interfaced Class of Silicon Electronics for Mapping Cardiac Electrophysiology. *Sci. Transl. Med.* **2010**, *2*, 24ra22.

(19) Kim, D.-H.; Lu, N. S.; Ghaffari, R.; Kim, Y.-S.; Lee, S. P.; Xu, L.; Wu, J.; Kim, R.-H.; Song, J.; Liu, Z.; Viventi, J.; de Graff, B.; Elolampi, B.; Mansour, M.; Slepian, M. J.; Hwang, S.; Moss, J. D.; Won, S.-M.; Huang, Y.; Litt, B.; et al. Materials for Multifunctional Balloon Catheters with Capabilities in Cardiac Electrophysiological Mapping and Ablation Therapy. *Nat. Mater.* **2011**, *10*, 316−323.

(20) Xu, L.; Gutbrod, S. R.; Bonifas, A. P.; Su, Y.; Sulkin, M. S.; Lu, N.; Chung, H.-J.; Jang, K.-I.; Liu, Z.; Ying, M.; Lu, C.; Webb, R. C.; Kim, J.-S.; Laughner, J. I.; Cheng, H.; Liu, Y.; Ameen, A.; Jeong, J.-W.; Kim, G.-T.; Huang, Y.; et al. 3D Multifunctional Integumentary Membranes for Spatiotemporal Cardiac Measurements and Stimulation Across the Entire Epicardium. *Nat. Commun.* **2014**, *5*, 3329.

(21) Kim, D.-H.; Ghaffari, R.; Lu, N.; Wang, S.; Lee, S. P.; Keum, H.; D'Angelo, R.; Klinker, L.; Su, Y.; Lu, C.; Kim, Y.-S.; Ameen, A.; Li, Y.; Zhang, Y.; de Graff, B.; Hsu, Y.-Y.; Liu, Z.; Ruskin, J.; Xu, L.; Lu, C.; et al. Electronic Sensor and Actuator Webs for Large-Area Complex Geometry Cardiac Mapping and Therapy. *Proc. Natl. Acad. Sci. U. S. A.* **2012**, *109*, 19910−19915.

(22) Dai, X.; Zhou, W.; Gao, T.; Liu, J.; Lieber, C. M. Three-Dimensional Mapping and Regulation of Action Potential Propagation in Nanoelectronics Innervated Tissues. *Nat. Nanotechnol.* **2016**, *11*, 776−782.

(23) Jeong, J.-W.; McCall, J. G.; Shin, G.; Zhang, Y.; Al-Hasani, R.; Kim, M.; Li, S.; Sim, J. Y.; Jang, K. I.; Shi, Y.; Hong, D. Y.; Liu, Y.; Schmitz, G. P.; Xia, L.; He, Z.; Gamble, P.; Ray, W. Z.; Huang, Y.; Bruchas, M. R.; Rogers, J. A. Wireless Optofluidic Systems for Programmable *In Vivo* Pharmacology and Optogenetics. *Cell* **2015**, *162*, 662−674.

DOI: 10.1021/acsnano.8b05552
ACS Nano 2018, 12, 10317−10326

(24) Montgomery, K. L.; Yeh, A. J.; Ho, J. S.; Tsao, V.; Mohan Iyer, S.; Grosenick, L.; Ferenczi, E. A.; Tanabe, Y.; Deisseroth, K.; Delp, S. L.; Poon, A. S. Y. Wirelessly Powered, Fully Internal Optogenetics for Brain, Spinal and Peripheral Circuits in Mice. *Nat. Methods* **2015**, *12*, 969−974.
(25) Kim, T.; McCall, J. G.; Jung, Y. H.; Huang, X.; Siuda, E. R.; Li, Y.; Song, J.; Song, Y. M.; Pao, H. A.; Kim, R.-H.; Lu, C.; Lee, S. D.; Song, I.-S.; Shin, G.; Al-Hasani, R.; Kim, S.; Tan, M. P.; Huang, Y.; Omenetto, F. G.; Rogers, J. A.; et al. Injectable, Cellular-Scale Optoelectronics with Applications for Wireless Optogenetics. *Science* **2013**, *340*, 211−216.
(26) Canales, A.; Jia, X.; Froriep, U. P.; Koppes, R. A.; Tringides, C. M.; Selvidge, J.; Lu, C.; Hou, C.; Wei, L.; Fink, Y.; Anikeeva, P. Multifunctional Fibers for Simultaneous Optical, Electrical and Chemical Interrogation of Neural Circuits *In Vivo*. *Nat. Biotechnol.* **2015**, *33*, 277−284.
(27) Wilson, B. S.; Finley, C. C.; Lawson, D. T.; Wolford, R. D.; Eddington, D. K.; Rabinowitz, W. M. Better Speech Recognition with Cochlear Implants. *Nature* **1991**, *352*, 236−238.
(28) Bowman, L.; Meindl, J. D. The Packaging of Implantable Integrated Sensors. *IEEE Trans. Biomed. Eng.* **1986**, *BME-33*, 248−255.
(29) Sanders, R. S.; Lee, M. T. Implantable Pacemakers. *Proc. IEEE* **1996**, *84*, 480−486.
(30) Mayberg, H. S.; Lozano, A. M.; Voon, V.; McNeely, H. E.; Seminowicz, D.; Hamani, C.; Schwalb, J. M.; Kennedy, S. H. Deep Brain Stimulation for Treatment-Resistant Depression. *Neuron* **2005**, *45*, 651−660.
(31) Thejo Kalyani, N.; Dhoble, S. J. Novel Materials for Fabrication and Encapsulation of OLEDs. *Renewable Sustainable Energy Rev.* **2015**, *44*, 319−347.
(32) Park, J.-S.; Chae, H.; Chung, H. K.; Lee, S. I. Thin Film Encapsulation for Flexible AM-OLED: A Review. *Semicond. Sci. Technol.* **2011**, *26*, 034001.
(33) Ahmad, J.; Bazaka, K.; Anderson, L. J.; White, R. D.; Jacob, M. V. Materials and Methods for Encapsulation of OPV: A Review. *Renewable Sustainable Energy Rev.* **2013**, *27*, 104−117.
(34) Fang, H.; Zhao, J.; Yu, K. J.; Song, E.; Farimani, A. B.; Chiang, C.-H.; Jin, X.; Xue, Y.; Xu, D.; Du, W.; Seo, K. J.; Zhong, Y.; Yang, Z.; Won, S. M.; Fang, G.; Choi, S. W.; Chaudhuri, S.; Huang, Y.; Alam, M. A.; Viventi, J.; et al. Ultrathin, Transferred Layers of Thermally Grown Silicon Dioxide as Biofluid Barriers for Biointegrated Flexible Electronic Systems. *Proc. Natl. Acad. Sci. U. S. A.* **2016**, *113*, 11682−11687.
(35) Fang, H.; Yu, K. J.; Gloschat, C.; Yang, Z.; Song, E.; Chiang, C.-H.; Zhao, J.; Won, S. M.; Xu, S.; Trumpis, M.; Zhong, Y.; Han, S. W.; Xue, Y.; Xu, D.; Choi, S. W.; Cauwenberghs, G.; Kay, M.; Huang, Y.; Viventi, J.; Efimov, I. R.; et al. Capacitively Coupled Arrays of Multiplexed Flexible Silicon Transistors for Long-Term Cardiac Electrophysiology. *Nat. Biomed. Eng.* **2017**, *1*, 0038.
(36) Sze, S. M. *Semiconductor Devices: Physics and Technology*, 2nd ed.; John Wiley & Sons, Inc.: Hoboken, NJ, 2008; pp 183−184.
(37) Song, E.; Fang, H.; Jin, X.; Zhao, J.; Jiang, C.; Yu, K. J.; Zhong, Y.; Xu, D.; Li, J.; Fang, G.; Du, H.; Zhang, J.; Park, J. M.; Huang, Y.; Alam, M. A.; Mei, Y.; Rogers, J. A. Thin, Transferred Layers of Silicon Dioxide and Silicon Nitride as Water and Ion Barriers for Implantable Flexible Electronic Systems. *Adv. Electron. Mater.* **2017**, *3*, 1700077.
(38) Song, E.; Lee, Y. K.; Li, R.; Li, J.; Jin, X.; Yu, K. J.; Xie, Z.; Fang, H.; Zhong, Y.; Du, H.; Zhang, J.; Fang, G.; Kim, Y.; Yoon, Y.; Alam, M. A.; Mei, Y.; Huang, Y.; Rogers, J. A. Transferred, Ultrathin Oxide Bilayers as Biofluid Barriers for Flexible Electronic Implants. *Adv. Funct. Mater.* **2018**, *28*, 1702284.
(39) Kang, S.-K.; Hwang, S.-W.; Cheng, H.; Yu, S.; Kim, B. H.; Kim, J.-H.; Huang, Y.; Rogers, J. A. Dissolution Behaviors and Applications of Silicon Oxides and Nitrides in Transient Electronics. *Adv. Funct. Mater.* **2014**, *24*, 4427−4434.
(40) García-Saucedo, C.; Field, J. A.; Otero-Gonzalez, L.; Sierra-Álvarez, R. Low Toxicity of HfO_2, SiO_2, Al_2O_3 and CeO_2 Nanoparticles to the Yeast, Saccharomyces Cerevisiae. *J. Hazard. Mater.* **2011**, *192*, 1572−1579.
(41) Lee, C. D.; Hara, S. A.; Yu, L.; Kuo, J. T. W.; Kim, B. J.; Hoang, T.; Pikov, V.; Meng, E. Matrigel Coatings for Parylene Sheath Neural Probes. *J. Biomed. Mater. Res., Part B* **2016**, *104*, 357−368.
(42) Lee, K. Y.; Yu, K. J.; Kim, Y.; Yoon, Y.; Xie, Z.; Song, E.; Luan, H.; Feng, X.; Huang, Y.; Rogers, J. A. Kinetics and Chemistry of Hydrolysis of Ultrathin, Thermally Grown Layers of Silicon Oxide as Biofluid Barriers in Flexible Electronic Systems. *ACS Appl. Mater. Interfaces* **2017**, *9*, 42633−42638.
(43) Li, R.; Cheng, H.; Su, Y.; Hwang, S.-W.; Yin, L.; Tao, H.; Brenckle, M. A.; Kim, D.-H.; Omenetto, F. G.; Rogers, J. A.; Huang, Y. An Analytical Model of Reactive Diffusion for Transient Electronics. *Adv. Funct. Mater.* **2013**, *23*, 3106−3114.
(44) Jin, X.; Jiang, C.; Song, E.; Fang, H.; Rogers, J. A.; Alam, M. A. Stability of MOSFET-Based Electronic Components in Wearable and Implantable Systems. *IEEE Trans. Electron Devices* **2017**, *64*, 3443−3451.
(45) Burgess, T.; Baum, J. C.; Fowkes, F. M.; Holmstrom, R.; Shirn, G. A. Thermal Diffusion of Sodium in Silicon Nitride Shielded Silicon Oxide Films. *J. Electrochem. Soc.* **1969**, *116*, 1005−1008.
(46) Korol, V. Sodium-Ion Implantation into Silicon. *Physica status solidi (a)* **1988**, *110*, 9−34.
(47) Schaeffer, H. A.; Mecha, J.; Steinmann, J. Mobility of Sodium Ions in Silica Glass of Different OH Content. *J. Am. Ceram. Soc.* **1979**, *62*, 343−346.
(48) Sun, Y.; Rogers, J. A. Inorganic Semiconductors for Flexible Electronics. *Adv. Mater.* **2007**, *19*, 1897−1916.

DOI: 10.1021/acsnano.8b05552
ACS Nano 2018, 12, 10317−10326